Intrinsic gain switching in optically injected quantum dot laser lasing simultaneously from the ground and excited state

Lukasz Olejniczak,[1,2,*] Krassimir Panajotov,[1,3] Sebastian Wieczorek,[4] Hugo Thienpont,[1] and Marc Sciamanna[2]

[1]*Department of Applied Physics and Photonics, Brussels Photonics Team B-PHOT, Vrije Universiteit Brussel, B-1050 Brussels, Belgium*
[2]*SUPELEC, OPTEL and LMOPS EA 4423 (Lab. Matériaux Optiques, Photonique et Systémes), 2 rue Edouard Belin, 57070 Metz, France*
[3]*Institute of Solid State Physics, 1784 Sofia, Bulgaria*
[4]*Mathematics Research Institute, University of Exeter, Exeter EX4 4QF, UK*
**Corresponding author: lolejnic@b-phot.org*

Received July 13, 2010; revised September 11, 2010; accepted September 17, 2010; posted September 21, 2010 (Doc. ID 131550); published October 27, 2010

We analyze theoretically nonlinear dynamics of an optically injected two-mode quantum dot laser lasing simultaneously from the ground and excited states. We show that although the external optical signal is injected into the ground-state mode alone, it can lead to the generation of regular picosecond pulses and pulse packages in the intensity of the excited-state mode. Generation of regular streams of picosecond pulses is attributed to an intrinsic gain switching mechanism where the relaxation time is modulated by the oscillations in the occupation of the ground and excited energy states. © 2010 Optical Society of America

OCIS codes: 140.5960, 140.3520.

1. INTRODUCTION

Optically injected single-mode quantum well (QW) lasers show a rich variety of nonlinear behaviors including stable locking, bistability, excitability, various routes to chaos, etc. [1–4]. All these dynamics are well understood now and can be modeled by single-mode rate equations [4]. There are, however, circumstances in which the multimode dynamics has to be taken into account. A good example is the polarization dynamics of vertical-cavity surface-emitting lasers (VCSELs). Owing to the cylindrical symmetry of VCSELs, each single-transverse mode is associated with two orthogonal linearly polarized modes with frequency splitting of a few gigahertz. A comprehensive study of bifurcations in a model of a two-polarization mode VCSEL subject to orthogonal optical injection (polarization of the injected light is orthogonal to the one of the solitary VCSEL mode) has been presented in [5–7]. It unveiled bifurcations beyond those found in the single-mode models such as Hopf bifurcation on a two-mode solution and transcritical bifurcation between two- and single-mode solutions [6]. Another example is a QW edge emitting laser (EEL) supporting the emission of two longitudinal modes with terahertz frequency spacing achieved by a special cavity design [8]. Optical injection in such a two-color laser revealed the importance of torus bifurcation in the route to two-mode antiphase dynamics with short-pulse packages and optical chaos.

In this paper we undertake theoretical study of nonlinear dynamics induced by optical injection in another two-mode laser system, namely, quantum dot (QD) laser. In these devices, the finite number of QDs within the active region and the discrete energy structure of QDs can lead to saturation of the ground state (GS) already at moderate currents. As a result, the occupation of the excited states (ESs) grows with the current, and the laser can start to lase from these states, too. Simultaneous emission from both states has been demonstrated for a solitary QD laser in [9]. Also, it has been studied for a QD laser subject to optical feedback [10] and for dual-wavelength mode-locking [11].

In QD lasers, injected carriers attain the ES and then the GS with rates determined by the capture and relaxation times, respectively. Both times depend on the fixed parameter corresponding to the empty destination state, i.e., ES for the capture process and GS for the relaxation process, and on the actual occupation of the destination state (see Section 2 for more details). Here, we demonstrate that oscillations of the GS occupation caused by optical injection can lead to modulation of the relaxation time and, consecutively, to oscillations in the occupation of the ES. Ultimately, such modulation provides a gain switching mechanism and leads to the emission of picosecond pulses from the ES. We show that the repetition rate of such pulses is determined by the frequency of the GS mode intensity oscillations.

2. THEORETICAL MODEL

To account for the presence of the ES we extended the theoretical model presented in [12] in a similar fashion as in [13]. Furthermore, to allow lasing from both states, we added an equation for the field of the ES mode. In the model used here, carriers from the wetting layer (WL) are first being captured into the ES and then relax to the GS

[9]. Contrary to the case of a multi-mode QW EEL [8], in our QD laser model different modes are associated with separate reservoirs of carriers. These reservoirs are coupled through the relaxation process and are filled up in a cascade manner with different rates determined by the relaxation and capture times that depend on the actual occupation of the respective states. We assume that due to the large (terahertz) frequency spacing between the GS and ES the injected light interacts directly only with the GS mode. Nevertheless, the injected light can affect the uninjected ES mode indirectly by modifying the relaxation time depending on the actual occupation of the GS due to the Pauli blocking term. The complete set of equations reads

$$\frac{dE_{\mathrm{ES}}}{dt} = \frac{1}{2}v_g g_{\mathrm{ES}}\left(2f_{\mathrm{ES}} - 1 - \frac{\gamma_s}{v_g g_{\mathrm{ES}}}\right)(1+i\alpha)E_{\mathrm{ES}}, \tag{1}$$

$$\frac{dE_{\mathrm{GS}}}{dt} = \frac{1}{2}v_g g_{\mathrm{GS}}\left(2f_{\mathrm{GS}} - 1 - \frac{\gamma_s}{v_g g_{\mathrm{GS}}}\right)(1+i\alpha)E_{\mathrm{GS}} + i\Delta E_{\mathrm{GS}} + \gamma_s\sqrt{\frac{S_m}{\hbar\omega}}, \tag{2}$$

$$\frac{df_{\mathrm{WL}}}{dt} = \frac{J_{QD}}{q} - \gamma_n f_{\mathrm{WL}} - \frac{f_{\mathrm{WL}}(1-f_{\mathrm{ES}})}{\tau_c^0}, \tag{3}$$

$$\frac{df_{\mathrm{ES}}}{dt} = -\gamma_n f_{\mathrm{ES}} + \frac{f_{\mathrm{WL}}(1-f_{\mathrm{ES}})}{4\tau_c^0} - \frac{f_{\mathrm{ES}}(1-f_{\mathrm{GS}})}{\tau_o^0} - v_g\sigma(2f_{\mathrm{ES}}-1)\times|E_{\mathrm{ES}}|^2, \tag{4}$$

$$\frac{df_{\mathrm{GS}}}{dt} = -\gamma_n f_{\mathrm{GS}} + \frac{2f_{\mathrm{ES}}(1-f_{\mathrm{GS}})}{\tau_o^0} - v_g\sigma(2f_{\mathrm{GS}}-1)|E_{\mathrm{GS}}|^2. \tag{5}$$

Here, f_{WL}, f_{ES}, and f_{GS} describe the occupation probabilities or the numbers of carriers in the WL, ES, and GS, respectively, normalized to the product of the number of QDs and the degeneracy of the respective states. The degeneracy of the GS is 2 and of the ES is 4. The number of carriers in the WL is normalized to the number of QDs only.

$$I_{\mathrm{GS,ES}} = |E_{\mathrm{GS,ES}}|^2$$

represents the intensity of light emitted by the GS/ES mode. The carrier non-radiative decay rate is $\gamma_n = 1\ \mathrm{ns}^{-1}$, while the photon decay rate is $\gamma_s = 590\ \mathrm{ns}^{-1}$. The capture time $\tau_c = \tau_c^0/(1-f_{\mathrm{ES}})$ and relaxation time $\tau_o = \tau_o^0/(1-f_{\mathrm{GS}})$ are determined by the fixed values τ_c^0 and τ_o^0 corresponding to the empty ES and GS, respectively, and by the actual occupation of the ES and GS. The linewidth enhancement factor is $\alpha = 1.2$, the linear optical gain coefficient is $g_{\mathrm{GS}} = 72\ \mathrm{cm}^{-1}$ for the GS and $g_{\mathrm{ES}} = 2g_{\mathrm{GS}}$ for the ES, and the interaction cross section is $\sigma = 0.6\ \mathrm{nm}^2$. All these values are identical to those used in the original report on optically injected QD laser [12].

The pump current J_{QD} is normalized to the number of QDs. $v_g = 0.833\times10^8$ m/s is the group velocity, q is the electron charge, and $\hbar$ is the Planck constant. The injected signal is characterized by its frequency detuning from the GS mode, Δ, and strength S_m (energy density of the injected light). The frequency of the master laser amounts to $\omega = 1.45\times10^{15}\ \mathrm{s}^{-1}$.

To facilitate numerical calculations, we rewrite Eqs. (1)–(5) in a dimensionless form using the normalized field $F_{\mathrm{GS,ES}} = E_{\mathrm{GS,ES}}\sqrt{v_g\sigma/\gamma_n}$, the normalized gain coefficient $a_{\mathrm{GS,ES}} = (1/2)(v_g g_{\mathrm{GS,ES}}/\gamma_n)$, the normalized photon decay rate $\gamma_{\mathrm{GS,ES}} = \gamma_s/v_g g_{\mathrm{GS,ES}}$, the normalized pump current $J = J_{QD}/q\gamma_n$, the normalized capture rate to the empty ES $C^0 = 1/\tau_c^0$, the normalized relaxation rate to the empty GS $R^0 = 1/\tau_o^0$, the normalized detuning $\Delta' = \Delta/\gamma_n$, and $B = \gamma_s\sqrt{v_g\sigma/\hbar\omega\gamma_n^3}$. The time is normalized to the carrier decay rate γ_n, i.e., $t' = t\gamma_n$. Since the phase of the (uninjected) ES mode decouples from the rest of equations, Eq. (1) for the complex-valued amplitude E_{ES} can be replaced with an equation for the real-valued intensity I_{ES}. The final set of equations reads

$$\frac{dI_{\mathrm{ES}}}{dt'} = 2a_{\mathrm{ES}}(2f_{\mathrm{ES}} - 1 - \gamma_{\mathrm{ES}})I_{\mathrm{ES}}, \tag{6}$$

$$\frac{dF_{\mathrm{GS}}}{dt'} = a_{\mathrm{GS}}(2f_{\mathrm{GS}} - 1 - \gamma_{\mathrm{GS}})(1+i\alpha)F_{\mathrm{GS}} + i\Delta' F_{\mathrm{GS}} + B\sqrt{S_m}, \tag{7}$$

$$\frac{df_{\mathrm{WL}}}{dt'} = J - f_{\mathrm{WL}} - C^0 f_{\mathrm{WL}}(1-f_{\mathrm{ES}}), \tag{8}$$

$$\frac{df_{\mathrm{ES}}}{dt'} = -f_{\mathrm{ES}} + 0.25C^0 f_{\mathrm{WL}}(1-f_{\mathrm{ES}}) - R^0 f_{\mathrm{ES}}(1-f_{\mathrm{GS}}) - (2f_{\mathrm{ES}}-1)I_{ES}, \tag{9}$$

$$\frac{df_{\mathrm{GS}}}{dt'} = -f_{\mathrm{GS}} + 2R^0 f_{\mathrm{ES}}(1-f_{\mathrm{GS}}) - (2f_{\mathrm{GS}}-1)|F_{\mathrm{GS}}|^2. \tag{10}$$

Similarly to the original model [12], our extended model does not account for thermally induced escape of carriers. Even though both models can reproduce qualitatively well the experimental findings obtained at room temperature, they seem to be better suited to describe a QD laser operating in a low-temperature range [14]. This is because, in this regime, QDs are decoupled from the WL and each other so that the occupation of the GS increases with increasing the pump current; and, consequently, the laser can saturate to $f_{\mathrm{GS}} = 1$, which is not the case for devices operating at room temperature [14].

Analytical expressions for the steady state occupations of the GS and ES and the mode intensities in a free-running laser, i.e., without optical injection, are given in Appendix A. Those expressions were used to plot the mode intensity versus current for different values of the relaxation rate to the empty GS (R^0) in Fig. 1. As can be seen from the figure, the ES mode reaches its lasing threshold when the GS mode saturates. The threshold current for the ES mode strongly depends on the value of R^0. When R^0 decreases the ES mode starts to lase at smaller currents, while the threshold for the GS mode slightly increases. At extremely slow relaxation, i.e., $R^0 = 50$, the laser emits only the ES mode. For the remaining

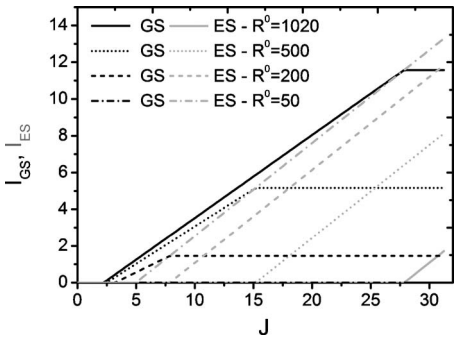

Fig. 1. Intensities of the GS (black) and ES (gray) modes versus current for different values of the relaxation rate to the empty *GS*.

part of the paper we fix $R^0=500$, giving the threshold current for the ES mode of $J_{th}^{ES}=15$, and $J_{th}^{ES}:J_{th}^{GS}=6:1$. This choice reflects the available experimental values [9,15].

3. INTRINSIC GAIN SWITCHING IN OPTICALLY INJECTED QUANTUM DOT LASER LASING SIMULTANEOUSLY FROM THE GROUND AND EXCITED STATES

In this section we fix the current to $J=17$ that is just above the lasing threshold of the ES mode in a free-running laser, and investigate injection-induced dynamics of the GS and ES modes. To give a rough overview of the dynamics, we present in Fig. 2(a) an "extrema map" where we use different shades of gray to indicate a number of different extrema in the time series of the ES mode intensity I_{ES} for each point in the (Δ,S_m) plane. Specifically, light gray L^1 indicates the absence of extrema and $I_{ES}=0$ (steady state solution with the ES mode below the threshold), light gray L^2 indicates the absence of extrema and $I_{ES}>0$ (steady state solution with the ES mode above the threshold), dark gray U^2 indicates two different extrema (period-1 periodic orbit), white U^3 indicates three different extrema, and gray $U^{>3}$ indicates more than three different extrema and includes cases of irregular possibly chaotic oscillations. Interestingly, optical injection into the GS mode can have various effects on the dynamics of the ES mode. Depending on the settings of Δ and S_m, it can stop lasing of the ES mode or excite (irregular) self-pulsations in the ES mode intensity.

While the GS mode always remains above the threshold, its intensity dynamics are limited to two types of locking and time-periodic oscillations. In a single-mode injected laser, locking is a single-frequency operation when the laser emits at the frequency of the injected signal. In two-mode lasers, however, it is possible to have two frequency operations with a locked injected mode and an unlocked uninjected one. Such a behavior has been observed with two polarization-mode QW VCSELs [6] and with two longitudinal-mode QW EELs [16].

In Fig. 2(a) different types of locking of the GS mode are represented by light gray regions L^1 and L^2, that is, single-frequency locking (when the ES mode is suppressed) exists inside L^1, and two-frequency locking (when the ES mode is unsuppressed and unlocked) exists inside L^2. We also used numerical continuation [17] to calculate a two-parameter bifurcation diagram for the same

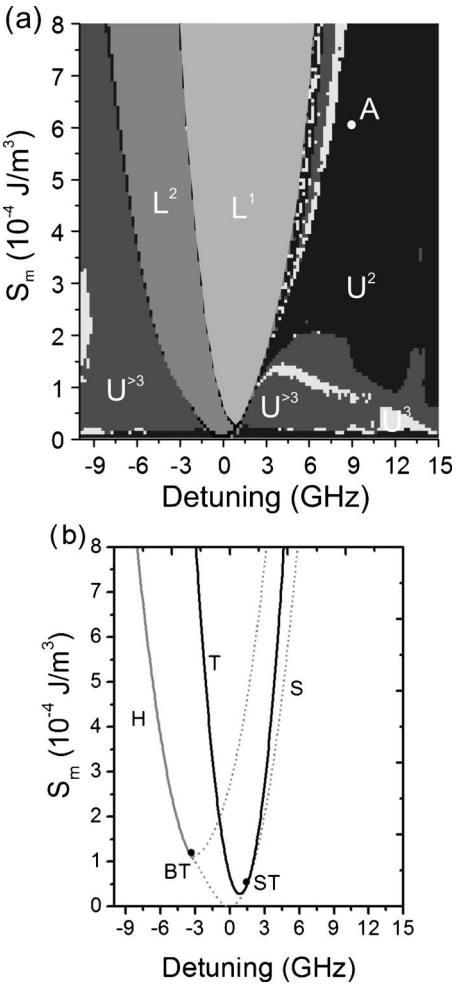

Fig. 2. (a) Extrema map for $J=17$. Representation of respective shades of gray: light gray L^1—locked GS mode and suppressed ES one (lack of extrema); light gray L^2—locked GS mode but unsuppressed ES one (lack of extrema); dark gray U^2—time-periodic pulsations (two extrema); white U^3—oscillations characterized by three extrema; gray $U^{>3}$—complex dynamics characterized by more than thee extrema, possibly chaotic. (b) Two-parameter bifurcation diagram calculated by AUTO [17]. Solid gray curve H denotes Hopf bifurcation, dotted gray curve S denotes saddle-node bifurcation, and solid black curve T denotes transcritical bifurcation. BT and ST are codimensional two points at which the saddle-node–Hopf bifurcation curves and saddle-node and transcritical bifurcation curves, respectively, are tangent.

parameter values as in Fig. 2(a). Bifurcation analysis in Fig. 2(b) reveals that in the (Δ,S_m) plane locking is bounded by Hopf (H) and saddle-node (S) bifurcations. Furthermore, the transition between the two different types of locking occurs via transcritical (T) bifurcation. This bifurcation defines the lasing threshold of the ES mode in the injected laser. For positive detuning Δ, the saddle-node bifurcation [curve S in Fig. 2(b)] takes place on a periodic orbit and is sometimes referred to as homoclinic saddle-node bifurcation [18]. As a result, the waveform of period-1 oscillations in the GS mode intensity found outside the locking region is influenced by a ghost of the saddle-node near the bifurcation and looks like deterministic self-pulsations described in [13].

The behavior of the ES mode in the unlocked region is much more diverse and complicated. First we investigate

its dynamics for the injection strength smaller than 2×10^{-4} J/m^3. The one-parameter bifurcation diagram for $S_m=1.5\times10^{-4}$ J/m^3 is shown in Fig. 3. Regardless of the detuning, the waveform of the ES mode has one extremum at zero-intensity level, meaning that it is pulsed, and the respective points in the bifurcation diagram correspond to the amplitudes of the pulses. A comparison between Figs. 3(a) and 3(b) reveals strong dependence on the sweeping direction of the detuning. Namely, starting from $\Delta=8.8$ GHz there is bistability between the pulsed output of the ES mode with periodic spikes of a fixed amplitude and the pulsed output of the ES mode that can be highly irregular and involve spikes of different amplitudes (as in region A in Fig. 3) or form more regular pulse patterns (as in region B in Fig. 3).

To characterize the dynamics of the modes for the injection strength larger than 2×10^{-4} J/m^3, we show in Fig. 4(a) the time traces of the GS and ES mode intensities for fixed injection parameters $S_m=6\times10^{-4}$ J/m^3, $\Delta=9$ GHz [point A in Fig. 2(a)]. As can be seen from this figure the ES mode fires periodic pulses at a constant amplitude, which is ten times higher than the maximum intensity of the GS mode. Temporal changes of the occupation of the respective energy states are shown in Fig. 4(b). Dynamics are governed by antiphase oscillations of the intensity and occupation of the GS caused by the optical injection. These oscillations modulate the relaxation time $\tau_o=\tau_o^0/(1-f_{GS})$ via the Pauli blocking term [see Fig. 4(c)]. Consequently, the occupation of the ES is also being modulated. In a similar way, oscillations of the occupation of the ES modulate the capture rate and influence the occupation of the WL. With the set of parameters used in the model, the GS is almost saturated, meaning that small changes in its occupation cause large changes in the relaxation time. The amplitude of such modulation is 0.5 ns. The amplitude of the capture time modulation is much smaller. The large increase in the relaxation time explains the considerable increase in the occupation of the ES (well above its threshold value $f_{ES}^{th}=0.72$) within the time corresponding to the increasing slope of the GS occupation in Fig. 4(b). The ES occupation is governed by

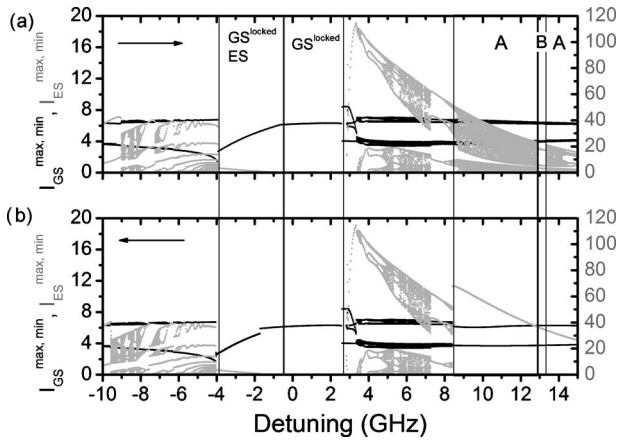

Fig. 3. One-parameter bifurcation diagram for $J=17$, $S_m=1.5\times10^{-4}$ J/m^3 when sweeping the detuning either (a) from negative to positive or (b) from positive to negative values. Black corresponds to the GS mode, whereas gray corresponds to the ES mode.

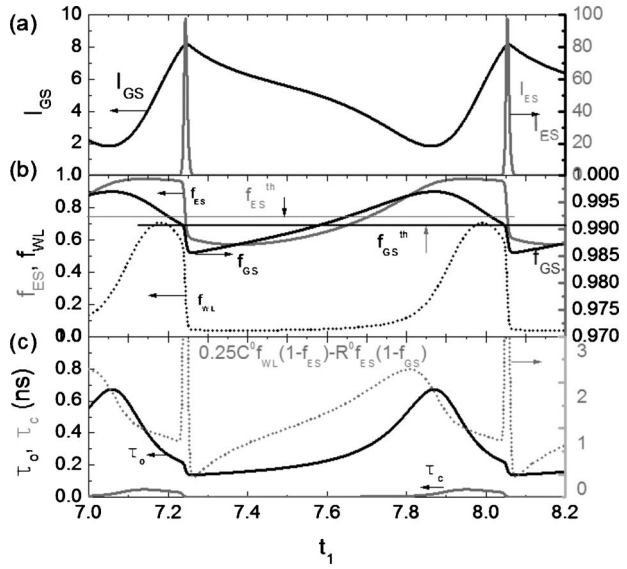

Fig. 4. Temporal evolution of (a) GS (left axis) and ES (right axis) mode intensities, and (b) occupation of the GS: solid black curve f_{GS} (right axis), ES: solid gray curve f_{ES} (left axis), and WL: dotted black curve f_{WL} (left axis). Horizontal black and gray lines represent threshold occupation of the GS and ES, respectively. (c) Modulation of the relaxation (black) and capture (gray) times resulting from changes in the occupation of the respective energy levels (left axis) and the difference between the capture $0.25C^0f_{WL}(1-f_{ES})$ and relaxation $-R^0f_{ES}(1-f_{GS})$ processes (dotted gray curve, right axis); $S_m=6\times10^{-4}$ J/m^3, $\Delta=9$ GHz.

the capture $0.25C^0f_{WL}(1-f_{ES})$ and relaxation $-R^0f_{ES}(1-f_{GS})$ processes in Eq. (9). The interplay of these two processes is plotted as a dotted light gray curve in Fig. 4(c). When the occupation of the GS and consequently the relaxation time start decreasing after achieving their maxima, the occupation of the ES still increases for some time because the capture to the ES dominates the process of relaxation to the GS. At some point the occupation of the ES saturates. When the decreasing occupation of the *GS* crosses its threshold value $f_{GS}^{th}=0.991$ the ES fires a large intensity pulse, while its occupation sharply decreases [the last stimulated emission term in Eq. (9)]. This resembles a typical gain switching mechanism and shows that modulation of the relaxation time can lead to generation of picosecond pulses.

In Fig. 5 the pulse duration and repetition rate are plotted as functions of the detuning. In the investigated

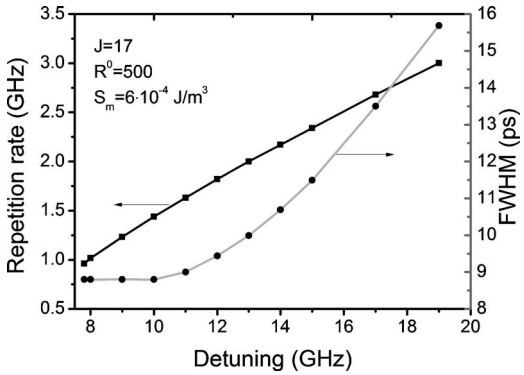

Fig. 5. Repetition rate (black) and the full width at half-maximum (gray) of pulses generated from the ES.

range, the pulse repetition rate increases linearly with the detuning and is of the order of a few gigahertz. At detuning of 8 GHz the pulse duration is as small as 8 ps. Similar values have been reported experimentally for pulses generated by a dual-wavelength mode-locked QD laser [11]. When the detuning increases, however, the pulses become broader.

For negative detuning, the locking region is bordered by parts of the saddle-node and Hopf bifurcation curves that meet together at the codimension-2 Bogdanov–Takens point BT [Fig. 2(b)]. The dynamics of the GS and ES modes in the unlocked region are characterized in Figs. 6–8.

Figure 6 depicts the two-mode Hopf bifurcation for large [Fig. 6(a)] and small [Fig. 6(b)] injection strengths. In close proximity to the Hopf bifurcation, the GS and ES modes oscillate in antiphase (not shown). As can be seen from Fig. 6 a number of extrema appear in the intensity of the ES mode when decreasing the detuning beyond the Hopf bifurcation point. What happens is that each time the ES mode raises above zero, its waveform follows relaxation oscillations (see also Fig. 8, graph 1). Comparing Figs. 6(a) and 6(b) one can conclude that the range of detuning corresponding to the pure antiphase oscillations of the GS and ES modes depends on the injection strength and shrinks when approaching the BT point.

Figure 7 presents forward and backward one-parameter bifurcation diagrams for the same injection strength as in Fig. 6(b), but for negative detuning reaching −50 GHz. As can be seen from this figure, the regular multipulse dynamics of the ES mode is followed by chaotic dynamics: region B in Fig. 7 (see also Figs. 8, graph 2). For even larger negative values of the detuning, regular pulses with two different amplitudes are generated (region D in Fig. 7). These periodic dynamics undergo period doubling cascade to chaos (region E in Fig. 7). Similarly to the scenario presented for positive detuning, there exists a region of bistability starting from the detuning of −13 GHz which extends over regions C_1–C_4 in Fig. 7. In region C_1 the bistability is between pulsed ES mode emissions with constant, but different amplitudes of pulses (see also Fig. 8, graph 3). In regions C_2 and C_3 one

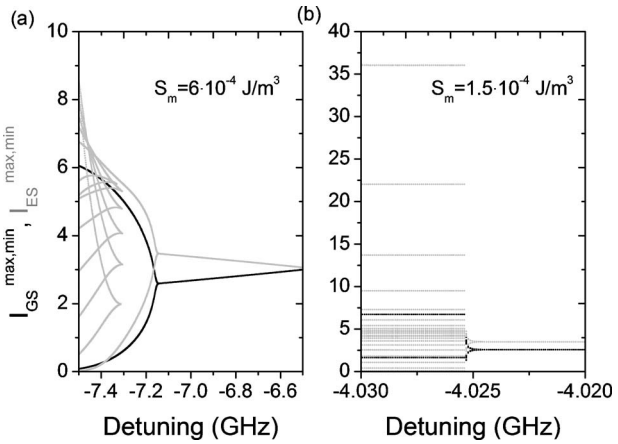

Fig. 6. One-parameter bifurcation diagram for (a) $S_m=6.0\times10^{-4}$ J/m^3 and (b) $S_m=1.5\times10^{-4}$ J/m^3 showing the behavior of the GS (black) and ES (gray) modes in close proximity to the two-mode Hopf bifurcation.

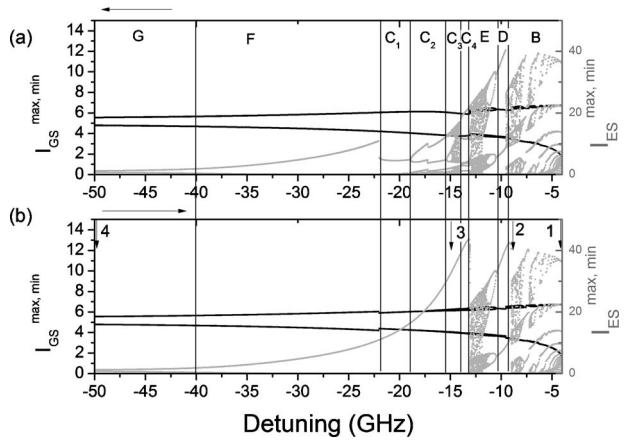

Fig. 7. One-parameter bifurcation diagram for $J=17$, $S_m=1.5\times10^{-4}$ J/m^3 for the GS (black) and ES (gray) modes, when sweeping the detuning either (a) from small to large or (b) from large to small negative values. Arrows 1–4 correspond to time traces in Fig. 8, graphs 1–4.

possible behavior is still associated with the pulsed ES mode emission with a constant amplitude of pulses [Fig. 7(b)], while the other one is associated with the emission of pulses which amplitudes undergo period doubling cascade to chaos when approaching region C_3 [Fig. 7(a)]. In region C_4 the bistability is between regular pulses with constant amplitude and multi-pulse pattern. In region F of Fig. 7 the ES mode fires pulses with a constant amplitude, and this amplitude becomes smaller and smaller as the detuning is increased. Finally, at the detuning larger than −40 GHz (region G in Fig. 7), the ES mode shows

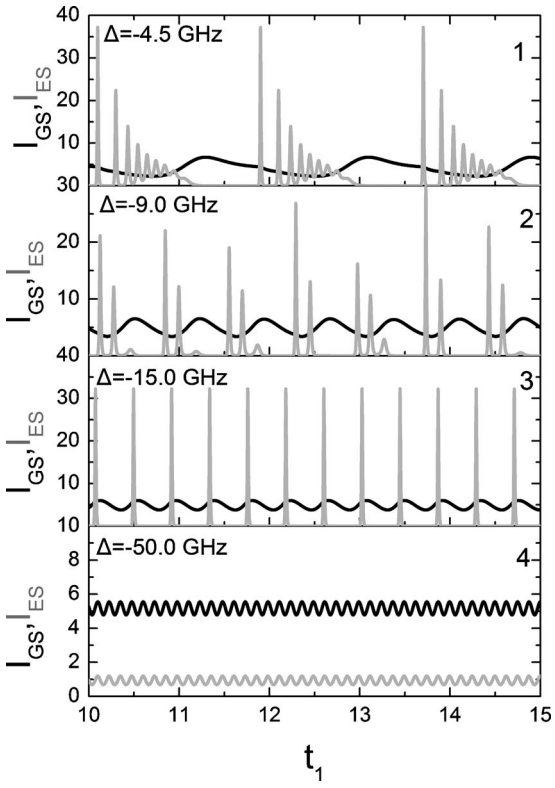

Fig. 8. Temporal evolution of the GS (black) and ES (gray) mode intensities for $S_m=1.5\times10^{-4}$ J/m^3 and 1: Δ=−4.5 GHz, 2: Δ=−9.0 GHz, 3: Δ=−15.0 GHz, 4: Δ=−50.0 GHz.

small amplitude oscillations that are in-phase with the oscillations of the GS mode as it is shown in Fig. 8, graph 4. Similar behavior is observed for large positive values of the detuning.

As long as the dynamics of the GS mode are limited to locking and period-1 time-periodic oscillations, the value of R^0 does not change the overall dynamics of the ES mode. It influences, however, the size of the respective regions in the injection parameter space.

4. GENERATION OF PULSE PACKAGES IN OPTICALLY INJECTED QUANTUM DOT LASER

The results presented so far suggest that modulation of the capture and relaxation times induced by optical injection can switch on and off the ES mode and consecutively result in the pulsating behavior of its intensity. It is therefore reasonable to check if such a pulsating behavior of the ES mode is maintained at higher currents. The extrema map computed for $J=20$ is presented in Fig. 9(a), and the corresponding bifurcation diagram is shown in Fig. 9(b).

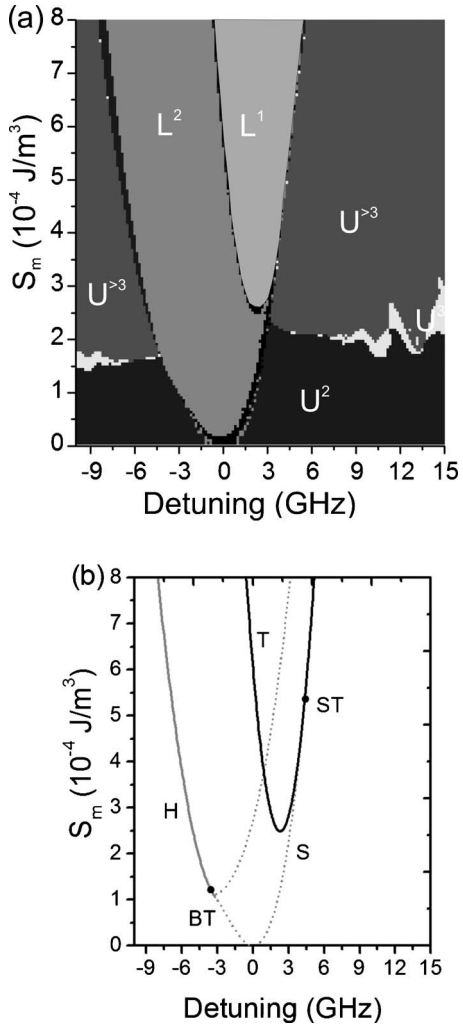

Fig. 9. (a) Extrema map for $J=20$. (b) Two-parameter bifurcation diagram calculated with AUTO [17]. The labeling and color coding are the same as in Fig. 2.

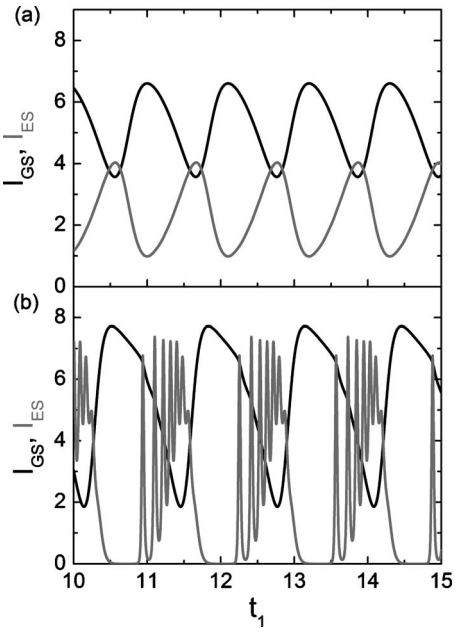

Fig. 10. Temporal evolution of the GS (black) and ES (gray) mode intensities for (a) $S_m=10^{-4}$ J/m^3, $\Delta=6$ GHz and (b) $S_m=4\times10^{-4}$ J/m^3, $\Delta=6$ GHz. $J=20$.

Comparing the two-parameter bifurcation diagrams in Figs. 2(b) and 9(b) one can conclude that at higher currents the region of locked single-frequency GS mode emission shrinks and is achievable at higher injection strengths. Similarly, the position of the codimension-2 saddle-node–transcritical tangency point ST moves to larger injection strengths, whereas the position of the codimension-2 Bogdanov–Takens point BT does not change. In the unlocked region regardless of the sign of the detuning, at the injection strength smaller than 2×10^{-4} J/m^3 both modes oscillate in antiphase [region U^2 in Fig. 10(a)]. At higher values of S_m, however, the waveform of the ES mode builds up by emission of short-pulse packages with decreasing depth of intensity modulation [region $U^{>3}$ in Fig. 10(b)]. The frequency of the spikes within the package corresponds to the relaxation oscillation frequency of the ES mode and is of the order of a few gigahertz. It is worth noticing that the two-mode QW EEL of [8] also shows the emission of pulse packages, but from both modes simultaneously.

At currents larger than $J=20$, the region of complex dynamics is attainable at a larger injection strength so that in the range of injection parameters investigated in this paper, the ES mode can either be suppressed, when the GS mode is locked, or can exhibit period-1 time-periodic oscillations. Such an emission already occurs at the current when $I_{GS}>I_{ES}$, which shows that the intensity ratio of the GS and ES mode emission does not influence the overall dynamics of the system.

5. CONCLUSIONS

This paper presents a theoretical study on optically injected quantum dot (QD) laser lasing simultaneously from the ground state (GS) and excited state (ES). External light is injected into the ground-state mode alone, and the

two lasing modes are coupled indirectly via the carrier relaxation process. We consider the range of currents where the ground- and excited-state modes lase simultaneously in the absence of optical injection.

Our studies unveil that, in the presence of optical injection, dynamics of the ground-state mode are limited to single-frequency locking (excited-state mode is suppressed), double-frequency locking (excited-state mode is unsuppressed), and unlocked time-periodic intensity oscillations. Inside the locking region defined in the plane of injection strength and frequency detuning, two different types of locking are separated by a transcritical bifurcation corresponding to the lasing threshold of the excited-state mode. Outside the locking region, the excited-state mode can exhibit very complicated behavior. Our studies focused on picosecond pulses generated by a gain switching mechanism that is associated with modulation of the relaxation time caused by the injection-induced oscillations in the occupation of the respective energy states. The model predicts that pulses as short as 8 ps are achievable. The repetition rate and duration of such pulses increase with the frequency detuning of the injected signal. At even higher currents, the region where the excited-state mode is suppressed and the ground-state mode is locked to the injected signal shrinks and requires higher injection strengths. Outside the locking region, the intensity of the excited-state mode is no longer pulsed, but it oscillates in antiphase with the intensity of the ground-state mode. For a certain set of injection parameters [region $U^{>3}$ in Fig. 9(a)], the envelope of the excited-state mode builds up by the emission of short-pulse packages with decreasing depth of modulation. The frequency of the spikes within the package corresponds to the relaxation oscillation frequency of the ES.

APPENDIX A

1. GS Emission Only

We present here steady state solutions of Eqs. (6)–(10) for a solitary QD laser, i.e., the time derivatives and the last two terms in Eq. (7) are set to zero. At the threshold for the GS mode emission, the GS gain balances the losses:

$$f_{GS} = \frac{\gamma_{GS} + 1}{2}. \tag{A1}$$

With the time derivatives at the left hand side of Eq. (8) put to zero, the steady state occupation of the WL reads

$$f_{WL} = \frac{J}{1 + C^0(1 - f_{ES})}. \tag{A2}$$

Similarly, putting to zero the time derivatives at the left hand side of Eq. (9) and then plugging in Eq. (A2) for f_{WL}, we obtain a quadratic equation for the steady state occupation of the ES, i.e.,

$$af_{ES}^2 + bf_{ES} + c = 0, \tag{A3}$$

where

$$a = C^0\left[1 + R^0\left(1 - \frac{\gamma_{GS} + 1}{2}\right)\right], \tag{A4}$$

$$b = -\left[4\left(R^0\left(1 - \frac{\gamma_{GS} + 1}{2}\right) + 1\right)(1 + C^0) + C^0 J\right], \tag{A5}$$

$$c = C^0 J. \tag{A6}$$

Only one solution, i.e., with $f_{ES} > 0$ is physical.

Knowing the steady-state occupations and putting to zero the time derivatives at the left hand side of Eq. (10), it is now possible to calculate the intensity of the GS mode, i.e., $|F_{GS}|^2$,

$$|F_{GS}|^2 = \frac{2R^0 f_{ES}(1 - f_{GS}) - f_{GS}}{\gamma_{GS}}. \tag{A7}$$

The current for which $|F_{GS}|^2$ equals to zero constitutes the threshold for the GS mode.

2. GS and ES Emission

In this case, both the GS and ES gains balance the corresponding losses, i.e.,

$$f_{GS} = \frac{\gamma_{GS} + 1}{2}, \tag{A8}$$

$$f_{ES} = \frac{\gamma_{ES} + 1}{2}. \tag{A9}$$

With the time derivatives at the left hand side of Eq. (8) put to zero and with known steady state occupation of the ES [Eq. (A9)], the steady state occupation of the WL reads

$$f_{WL} = \frac{J}{1 + C^0\left(1 - \frac{\gamma_{ES} + 1}{2}\right)}. \tag{A10}$$

The intensity of the GS mode is constant, given by Eq. (A7) together with Eqs. (A8) and (A9). The intensity of the ES mode, i.e., $|F_{ES}|^2$, can be calculated by putting to zero the time derivatives at the left hand side of Eq. (9):

$$|F_{ES}|^2 = \frac{0.25C^0 f_{WL}(1 - f_{ES}) - f_{ES} - R^0 f_{ES}(1 - f_{GS})}{\gamma_{GS}}. \tag{A11}$$

As for the occupations f_{GS}, f_{ES}, and f_{WL} in Eq. (A11), the steady state values calculated with Eqs. (A8)–(A10) should be used. The current for which $|F_{ES}|^2$ equals zero constitutes the threshold for the ES mode.

ACKNOWLEDGMENTS

The authors acknowledge the financial support of Conseil Regional de Lorraine, BELSPO IAP 6/10; Fonds voor Wetenschappelijk Onderzoek (FWO)–Vlaanderen; and Onderzoeksraand OZR-VUB for the GOA and IOF Projects, COST MP0702.

REFERENCES

1. R. Lang, "Injection locking properties of a semiconductor laser," IEEE J. Quantum Electron. **18**, 976–983 (1982).
2. T. B. Simpson, J. M. Liu, and A. Gavrielides, "Small-signal

analysis of modulation characteristics in a semiconductor laser subject to strong optical injection," IEEE J. Quantum Electron. **32**, 1456–1468 (1996).
3. T. B. Simpson, J. M. Liu, and A. Gavrielides, "Bandwidth enhancement and broadband noise reduction in injection-locked semiconductor lasers," IEEE Photon. Technol. Lett. **7**, 709–711 (1995).
4. S. Wieczorek, B. Krauskopf, T. B. Simpson, and D. Lenstra, "The dynamical complexity of optically injected semiconductor lasers," Phys. Rep. **416**, 1–128 (2005).
5. M. Sciamanna and K. Panajotov, "Route to polarization switching induced by optical injection in vertical-cavity surface-emitting lasers," Phys. Rev. A **73**, 023811 (2006).
6. M. Nizette, M. Sciamanna, I. Gatare, H. Thienpont, and K. Panajotov, "Dynamics of vertical-cavity surface-emitting lasers with optical injection: a two-mode model approach," J. Opt. Soc. Am. B **26**, 1603–1613 (2009).
7. I. Gatare, M. Sciamanna, M. Nizette, and K. Panajotov, "Bifurcation to polarization switching and locking in vertical-cavity surface-emitting lasers with optical injection," Phys. Rev. A **76**, 031803(R) (2007).
8. S. Osborne, A. Amann, K. Buckley, G. Ryan, S. P. Hegarty, G. Huyet, and S. O'Brien, "Antiphase dynamics in a multimode semiconductor laser with optical injection," Phys. Rev. A **79**, 023834 (2009).
9. A. Markus, J. X. Chen, C. Paranthoen, A. Fiore, C. Platz, and O. Gauthier-Lafaye, "Simultaneous two-state lasing in quantum-dot lasers," Appl. Phys. Lett. **82**, 1818–1820 (2003).
10. E. A. Viktorov, P. Mandel, I. O'Driscoll, O. Carroll, G. Huyet, J. Houlihan, and Y. Tanguy, "Low-frequency fluctuations in two-state quantum dot lasers," Opt. Lett. **31**, 2302–2304 (2006).
11. M. A. Cataluna, D. I. Nikitichev, S. Mikroulis, H. Simos, C. Simos, Ch. Mesaritakis, D. Syvridis, I. Krestnikov, D. Livshits, and E. U. Rafailov, "Dual-wavelength mode-locked quantum-dot laser, via ground and excited state transitions: experimental and theoretical investigation," Opt. Express **18**, 12832–12838 (2010).
12. D. Goulding, S. P. Hegarty, O. Rasskazov, S. Mielnik, M. Hartnett, G. Greene, J. G. McInerney, D. Rachinskii, and G. Huye, "Excitability in a quantum dot semiconductor laser with optical injection," Phys. Rev. Lett. **98**, 153903 (2007).
13. L. Olejniczak, K. Panajotov, H. Thienpont, and M. Sciamanna, "Self-pulsations and excitability in optically injected quantum dot lasers: impact of the excited states and spontaneous emission noise," Phys. Rev. A **82**, 023807 (2010).
14. D. R. Matthews, H. D. Summers, P. M. Smowton, and M. Hopkinson, "Experimental investigation of the effect of wetting-layer states on the gain–current characteristic of quantum-dot lasers," Appl. Phys. Lett. **81**, 4904–4906 (2002).
15. K. Gündoğdu, K. C. Hall, T. F. Boggess, D. G. Deppe, and O. B. Shchekin, "Ultrafast electron capture into p-modulation-doped quantum dots," Appl. Phys. Lett. **85**, 4570–4572 (2004).
16. S. Osborne, K. Buckley, A. Amann, and S. O'Brien, "All-optical memory based on the injection locking bistability of a two-color laser diode," Opt. Express **17**, 6293–6300 (2009).
17. E. Doedel, T. Fairgrieve, B. Sandstede, A. Champneys, Yu. Kuznetsov, and X. Wang, Auto-07p, http://indy.cs.concordia.ca/auto/.
18. S. H. Strogatz, *Nonlinear Dynamics and Chaos: With Applications in Physics, Biology, Chemistry, and Engineering* (Perseus Books, 1994).